Crystal Growth

Morphology Control of Stolzite Microcrystals with High Hierarchy in Solution**

Biao Liu, Shu-Hong Yu, Linjie Li, Qiao Zhang, Fen Zhang, and Ke Jiang*

The shape, phase, and size of inorganic nanocrystals are important elements in varying their electrical, optical, and other properties,[1] so rational control over these elements has become a hot research topic in recent years.[2] Much effort has been made in the design of rational methods for synthesizing one-dimensional nanostructures such as nanorods, nanowires,[3] nanobelts,[4] and nanotubes.[5] Self-assembled hierarchical and repetitive superstructures are also fascinating because of their promising complex functions.[6] Chemical vapor deposition (CVD),[4,7] laser-assisted catalytic growth (LCG),[8] the use of hard templates,[9] electrochemical deposition, and controlled solution growth at elevated temperature or pH value are general synthesis routes.[5] Application of organic additives,[10] self-assembled organic superstructures, and templates with complex functionalization patterns[11] to direct the growth of inorganic material is also attractive, as controlled morphologies and architectures can be obtained under near-natural conditions.[12]

Lead tungstate ($PbWO_4$) has attracted intense interest for its scintillator applications in high-energy physics.[13] This crystal has a density of 8.2 $g\,cm^{-3}$, a short decay time (less than

[*] B. Liu, Prof. Dr. S.-H. Yu, L. Li, Q. Zhang, F. Zhang, K. Jiang
Department of Nanomaterials and Nanochemistry
Hefei National Laboratory for Physical Sciences at Microscale
Structure Research Laboratory of CAS and
Department of Materials Science and Engineering
University of Science and Technology of China
Hefei 230026 (P. R. China)
Fax: (+86) 551-360-3040
E-mail: shyu@ustc.edu.cn

[**] This work was supported by special funding from the Centurial Program of the Chinese Academy of Sciences, the Distinguished Youth Fund (Contract No. 20325104), the Distinguished Team (Grant No. 20321101), and Contract No. 50372065 from the Natural Science Foundation of China.

Supporting information for this article is available on the WWW under http://www.angewandte.org or from the author.

 DOI: 10.1002/ange.200460090

10 ns for 85% of light output), and high resistance to radiation damage (10^7 rad for undoped material and 10^8 rad for La-doped $PbWO_4$).[14] Since 1994 it has been used as a scintillating medium for a new-generation crystal calorimeter in the Large Hadron Collider (LHC) project at CERN.[15] Moreover, $PbWO_4$ is promising as an active medium in laser and stimulated Raman scattering.[16]

A lot of effort has been made to synthesize $PbWO_4$ crystals. Single crystals are usually grown from the melt by the Czochralski[13] and Bridgeman[14] methods, whereas a hydrothermal route results in $PbWO_4$ crystals with poorly defined shapes.[17] Recently, $CdWO_4$ and $PbWO_4$ nano- and microcrystals with various morphologies such as rods, spindles, and pagodas were synthesized by a wet chemical route.[18,19] Nitsch et al. synthesized $PbWO_4$ with a scheelite structure from a gel at low temperature.[20]

Herein, we introduce a facile and mild solution method for preparing $PbWO_4$ crystals with controlled morphologies and special optical properties. Tetragonal stolzite with hierarchical microstructures can be easily synthesized on a large scale by controlling the reaction conditions, such as pH value, surfactant, and temperature.

Figure 1 shows the X-ray diffraction (XRD) patterns of the as-prepared products at different temperatures and pH values with the same initial concentrations (the concentrations of Pb^{2+}, WO_4^{2-}, and cetyltrimethylammonium bromide (CTAB) were all 0.0333 mol L^{-1}). The reflection peaks of the different products can be indexed as a pure tetragonal scheelite structure with cell parameters $a = 5.46$ and $c = 12.04$ Å, which is in good agreement with the literature values (JCPDS Card Number 86-0843). However, on comparing the peak intensities we found that the relative intensity of the peaks corresponding to the (004) and (200) planes varied significantly from the literature value, which indicates the different tropism of the crystals.

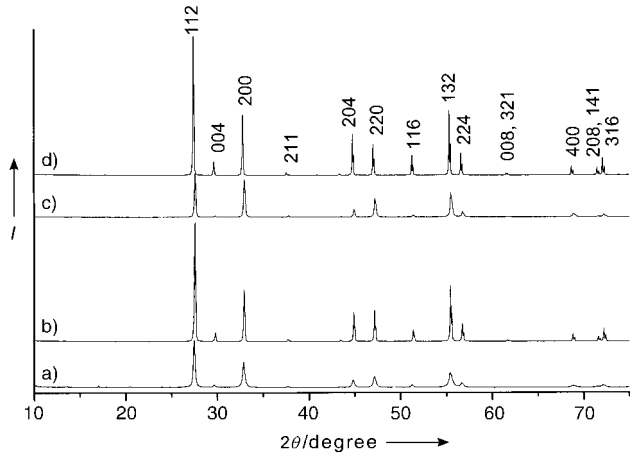

Figure 1. XRD patterns of the $PbWO_4$ obtained under different conditions: a) aging at 60 °C for 60 h, pH 4.0; b) aging at 60 °C for 18 h, pH 7.0; c) aging at 160 °C for 12 h, pH 4.0; d) aging at 160 °C for 12 h, pH 7.0. The initial concentrations of CTAB, Pb^{2+}, and WO_4^{2-} were all 0.0333 mol L^{-1}.

Figure 2a is a typical SEM image of the sample (Figure 1a) obtained after aging at 60 °C for 60 hours, which shows that the product consists of homogeneous spindlelike microrods of diameter 0.8–1.5 μm at the center and length more than 10 μm. High-magnification SEM images (Figure 2b–d) clearly reveal that the microrods are constructed from ellipsoidal particles with a diameter of about 100 nm and length of about 1 μm. It is interesting that these ellipsoidal nanoparticles are highly directed to form arrays in a somewhat helical manner (see the arrows in Figure 2b,c). Our proposed schematic illustration for such complex structures is depicted in Figure 2d.

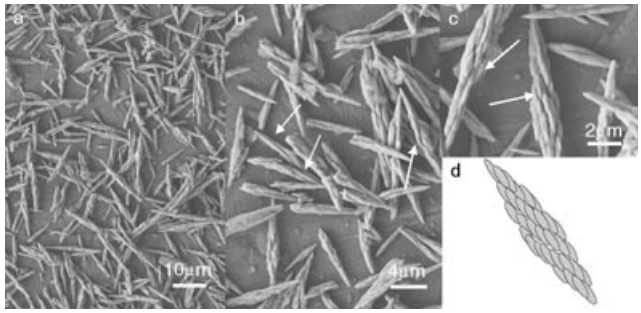

Figure 2. a)–c) SEM images of the $PbWO_4$ helixlike structures obtained by aging at 60 °C for 60 h; the concentrations of Pb^{2+}, WO_4^{2-}, and CTAB were all 0.0333 mol L^{-1}, pH 4.0. The arrows show helixlike structures which are composed of arrayed ellipsoidal particles. d) A schematic illustration of the helixlike structures.

The growth process of these helical structures was carefully followed by time-dependent experiments. The TEM image in Figure 3a shows that some spindles and chainlike structures occur. These structures are composed of directly arrayed nanopolyhedrons (Figure 3b,d) that are attached to each other in an interesting parallel and scalariform way, rather than in a simple parallel manner. Selected-area electron diffraction (SAED) and high-resolution TEM (HRTEM) were used to investigate how the nanopolyhedrons are attached to each other. Figure 3c shows the electron diffraction (ED) patterns recorded from the whole chainlike structure (Figure 3b), which can be indexed to tetragonal-phase $PbWO_4$ viewed along the $[28\bar{1}]$ direction. Similarly, the ED patterns (Figure 3d) recorded from the whole spindle constructed from assembled nanopolyhedrons (Figure 3e) can be indexed to tetragonal-phase $PbWO_4$ viewed along the $\langle 1\bar{1}0 \rangle$ direction. The ED patterns are similar from whichever direction they are viewed or from whichever congeries in the samples they are recorded, which underlines the fact that the attached nanoparticles share the same crystal direction. This observation was further confirmed by a careful HRTEM study. Therefore, the early stage in the formation of such helixlike structures still agrees well with that of the final stage (Figure 2).

The two-dimensional crystal-lattice patterns are the same even though they are obtained from the "subunits" of the crystals, that is, different nanopolyhedrons (Figure 3e–h). The fringe spacing along the different directions was determined

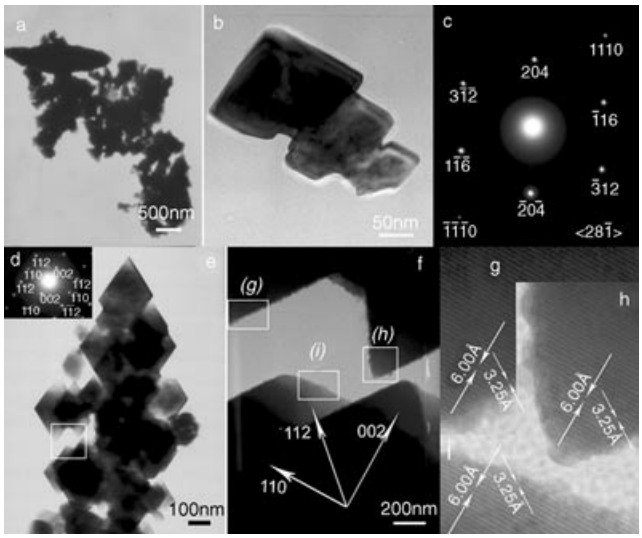

Figure 3. TEM images, ED patterns, and HRTEM images of the sample obtained in the early stages of forming $PbWO_4$ helical structures by mixing $Na_2WO_4{\cdot}2H_2O$, $PbAc_2$, and CTAB solution. The concentrations of Pb^{2+}, WO_4^{2-}, and CTAB were all kept at 0.0333 mol L^{-1}, pH 4.0. a) The general morphology of the sample. b) The chainlike structure formed by nanopolyhedrons assembled in a scalariform manner, which is observed frequently in the sample. c) The ED pattern recorded from the whole chainlike structure shown in (b). d) The ED pattern recorded from the whole spindlelike particle shown in (e). e) A typical spindlelike particle which is constructed from assembled nanopolyhedrons, showing the scalariform ordered assembly. f) A HRTEM image taken from the area marked by the pane in (e). g)–i) HRTEM images magnified from (f); the areas are indicated by the panes marked with *(g)*, *(h)*, and *(i)*.

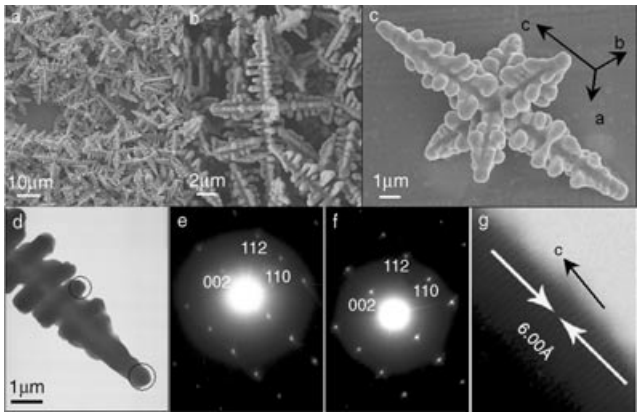

Figure 4. SEM images, TEM images, and ED patterns of the $PbWO_4$ dendrites obtained after aging at 60 °C for 18 h. The initial concentrations of Pb^{2+}, WO_4^{2-}, and CTAB were all 0.0333 mol L^{-1}, pH 7.0. a) A general view of the sample; b) a higher magnification SEM image; c) a typical single dendrite; d) a magnified TEM image showing part of the dendrite; e) ED pattern recorded from the branched part marked with circles in (d); f) ED pattern recorded from the tip of the trunk circled in (d); g) a typical HRTEM image taken from the tip of the branch.

as 3.25 and 6.00 Å for the (112) and (002) planes, respectively. It can be concluded that the elongated helical structures evolved from such aggregates, which grew preferentially along the *c* axis after aging for some time. The nanopolyhedrons were formed quickly after the reagents were mixed, and the spindles with hierarchical structures evolved from the nanopolyhedrons by the oriented attachment process accompanying Ostwald ripening. Such events are consistent with previous reports[21–23] of a so-called "oriented attachment" process that controls the initial stages in the formation of these unusual structures. However, the Ostwald ripening process also contributes to the formation of such structures, by "shearing" the nanopolyhedrons into the blunt ellipsoidal particles identified in their ripened final stage.

The morphology of the products varied greatly when the pH value was increased to 7.0 and the other conditions were kept the same. All the samples are homogeneous dendritic structures (Figure 4 a,b), which are quite similar to that reported for cubic PbS microstructures.[24,25] However, the individual $PbWO_4$ dendrite with three-dimensional structure displays more complex features than that previously reported for PbS.[24,25] There are two shorter trunks and a longer one; three crossed trunks construct the framework in a perfect perpendicular manner. Four branches grow vertically on each trunk in two perpendicular directions, which are similar to the growth directions of the other two trunks, and ordered microrods parallel to each other form the branches. The length of the longer trunk is about 20 μm and that of the two branches is about 9 μm. The ratio of the lengths of the three main trunks is equal to the ratio of the cell parameters $c/a = c/b = 2.2{:}1$; therefore, it is believed that the longer trunk grew in the *c* direction and the two shorter ones, in the *a* or *b* direction (Figure 4 c). The dimensions of such high hierarchical structures finely reflect the outside embodiment of the intrinsic cell structure of stolzite quite well. Further optimization of the growth conditions could make it possible to obtain perfect hierarchical structures.

The structural characteristics of the crystal were further elucidated by TEM and ED techniques. The SAED patterns taken from the branch and main trunk areas marked by the circles in Figure 4 d (Figure 4 e,f, respectively) are identical, which indicates that they share the same crystal direction along the *c* axis. We also investigated some other crystals in the sample and found that this observation is universal for all dendritic crystals. A typical HRTEM image recorded from the tip of a branch is shown in Figure 4 g. The fringe spacing was about 6.00 Å, which corresponds to the lattice spacing for the (002) faces. This result confirmed the supposition of the growth direction of the dendritic crystal.

The temperature was found to significantly affect the shape of the particles. The shape when the temperature was increased to 160 °C and the other conditions were kept constant was completely different from that observed at low temperature. After hydrothermal treatment for 12 hours at 160 °C (pH 4.0), the products are dendritic structures (Figure 5 a,b), whose length ranges from several micrometers to more than 10 μm. Unlike the sample obtained at 60 °C for 60 hours, the individual $PbWO_4$ dendrite has only one trunk and four shrunken branches. The branches are perpendicular to the trunk and they are built up of parallel-arrayed particles. The sample was transformed into peanutlike microrods with certain crystal faces exposed (Figure 5 c,d) after hydrothermal treatment for 12 hours at pH 7.0.

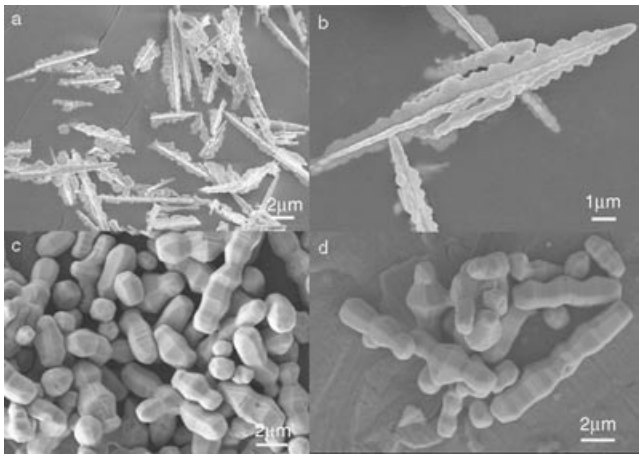

Figure 5. The influence of the pH value on the shape of $PbWO_4$ crystals. SEM images of: a),b) dendrite structures obtained at pH 4.0; c),d) rodlike and crosslike structures obtained at pH 7.0. Both of these samples were hydrothermally treated at 160 °C for 12 h, and the initial concentrations of Pb^{2+}, WO_4^{2-}, and CTAB were all 0.0333 mol L^{-1}.

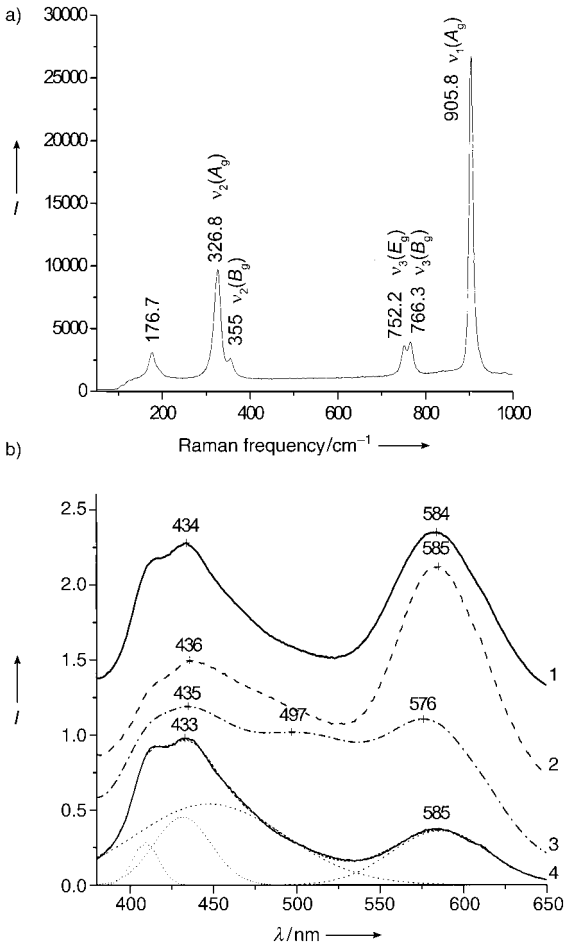

Figure 6. Optical properties of $PbWO_4$ crystals. a) Raman spectrum of the dendritic crystals with three trunks. b) Photoluminescence spectra. Curve 1 corresponds to the helical-array structure (Figure 2). Curve 2 corresponds to the dendritic structure with three trunks (Figure 4) and curve 3, to the dendritic crystals with only one trunk (Figure 5 a,b). Curve 4 corresponds to the peanutlike crystals (Figure 5 c,d) and is decomposed into four Gaussian components with peaks located at 410, 431, 454, and 485 nm (dotted lines). The excitation wavelength was 350 nm and all the spectra were recorded at room temperature.

Furthermore, the surfactant CTAB plays an important role in controlling the morphology of $PbWO_4$. If the other conditions are kept the same but with no added CTAB, or the concentration of CTAB is increased from 0.0333 to 0.2333 mol L^{-1}, only irregular particles are obtained (see Supporting Information). This observation can be explained if CTAB is adsorbed on specific facets of the $PbWO_4$ crystal and changes their surface energy if the amount of CTAB is appropriate. In contrast, the nonadsorbed facets will grow rapidly, as identified in the synthesis of TiO_2 nanocrystals controlled by a surfactant.[23] If the concentration of CTAB is too high, all the facets will have adsorbed surfactant such that it loses the ability to control the morphology of the growing crystals (see Supporting Information). We assume that the influence of the temperature and pH value on the growth of the crystals may lie in three aspects: affecting the adsorption of CTAB to different facets, changing the relative energy of the different facets, and affecting the controlling growth mechanism. More careful investigation is still needed.

The optical properties of these complex structures were also studied. The Raman spectrum of the stolzite helical structure (Figure 6 a) shows six bands in the range 100–1000 cm^{-1}. The peaks located at 905.8, 766.3, 752.2, 355, and 326.8 cm^{-1} correspond to the vibration modes $\nu_1(A_g)$, $\nu_3(B_g)$, $\nu_3(E_g)$, $\nu_2(B_g)$, and $\nu_2(A_g)$, respectively, which are consistent with those reported by Frost and co-workers.[26] However, a peak at 176.1 cm^{-1} was observed, which was not reported previously.[26] This peak is not assigned by Ross,[27] but it could be assigned as the translation mode analogous to that for $CdMoO_4$.[26] The two bands at 752.2 and 766.3 cm^{-1} are of almost identical intensity, which could be a consequence of identical crystal growth along the *a* and *b* axes. The Raman spectra of stolzite crystals with other shapes (Figure 5 and Supporting Information) are similar to that of the stolzite with hierarchical structures (Figure 2 and Figure 4).

Figure 6 b shows the room-temperature photoluminescence spectra of the different microstructures. Curves 1–4 correspond to the helical-array structures (Figure 2), the dendritic structures with three trunks (Figure 4), the dendritic structures with one trunk (Figure 5 a,b), and the peanutlike structures (Figure 5 c,d), respectively. All the curves have two main peaks: one is located at about 435 nm, which is similar to the reported value for the blue emission component;[13,28] the other is at about 585 nm and has never been observed previously in the bulk stolzite by other authors. The existence of the orange emission peak (at about 585 nm) may be related to the surface defects of the stolzite crystals, since it was observed in all the crystals with different structures as their size decreased to the micrometer scale but not in bulk crystals. Meanwhile, the relative intensities of the two broadening emission peaks seem closely related to the surface/volume ratio. The dendritic structures with three trunks have the biggest surface/volume ratio, and the relative intensity of the peak at 585 nm is highest. In contrast, the relative intensity of the emission peak at 585 nm for peanutlike structures, which

have the smallest surface/volume ratio, is the lowest. As described previously,[27a] the peaks at about 435 nm can be decomposed into several Gaussian components with peaks at 410, 431, 454, and 500 nm. The relative intensity of these decomposed peaks differed according to the particular crystal structure. For example, only the dendritic structures with one trunk give a strong peak at about 500 nm, and the helical-array structures give a stronger peak than the other structures at 435 nm. These results could indicate that the special structures might have some significant influence on the optical properties of tetragonal $PbWO_4$ crystals, which could be adopted in fine-tuning the surface-defect-related optical properties of this material.

In summary, we have successfully synthesized tetragonal $PbWO_4$ microcrystals with special hierarchical structures by controlling the solution reaction conditions, such as the amount of cationic surfactant CTAB, pH value, and temperature. The formation of helixlike structures has been investigated, and the oriented attachment process clearly contributes to the creation of such structures. Novel dendrites with hierarchical structures and exhibiting high crystal symmetry can be synthesized by further varying the pH value of the solution. Each dendritic crystal is composed of three main trunks on which four branches of arrayed nanorods start to grow. The CTAB and the temperature play important roles in controlling the morphology.

The optical properties of these hierarchical tetragonal $PbWO_4$ microcrystals differ from those of the bulk crystals, which could be related to their structural complexity and specialty. Further detailed characterization of this relationship is needed. Lead tungstate has an important role as a functional material, and thus the rational design of its complex structures could be of significance in scintillator applications. This synthesis method has demonstrated that it is possible to design complex and hierarchical structures by a facile, mild solution approach, which could be extended to the morphogenesis of other inorganic crystals with complex forms.

Experimental Section

Analytical grade $Na_2WO_4{\cdot}2H_2O$, $Pb(CH_3COO)_2$ ($PbAc_2$), and cetyltrimethylammonium bromide (CTAB) were purchased from Shanghai Chemical Industrial Company and were used without further purification. The reaction was carried out in a 60-mL teflon-lined stainless-steel autoclave or a 100-mL glass jar, and the temperature was regulated by a digital-type temperature-controlled oven.

Typical procedure: $Na_2WO_4{\cdot}2H_2O$ (2 mmol) and $PbAc_2$ (2 mmol) were placed in separate beakers, distilled water (25 mL) was added, and the contents were magnetically stirred to form homogeneous solutions at room temperature. The $PbAc_2$ solution was added slowly to the Na_2WO_4 solution under strong magnetic stirring to form a mixture containing amorphous particulates. The pH was adjusted to a specific value using NaOH or acetic acid solution (1 mol L^{-1}). The resulting precursor suspension was transferred to a teflon-lined stainless-steel autoclave (reaction temperature higher than 100 °C) or glass jar (reaction temperature lower than 100 °C). The container was sealed and maintained at a certain temperature for the desired reaction time, then allowed to cool slowly to room temperature. The products were collected by filtration, washed several times with distilled water and absolute ethanol, and finally dried in a vacuum at 60 °C for 4 h.

The products were characterized by X-ray diffraction (XRD), recorded on a MAC Science Co. Ltd. MXP 18 AHF X-ray diffractometer with monochromatized CuK_α radiation ($\lambda =$ 1.54056 Å). Microscopy was performed with a Hitachi (Tokyo, Japan) H-800 transmission electron microscope (TEM) at an accelerating voltage of 200 kV, and a JEOL-2010 high-resolution TEM, also at 200 kV. Raman spectra were recorded on a Jobin Yvon (France) LABRAM-HR confocal laser micro-Raman spectrometer at room temperature and an excitation wavelength of 514.5 nm. The photoluminescence spectra were recorded on a Fluorolog3-TAU-P instrument at room temperature.

Received: March 23, 2004

Keywords: self-assembly · crystal growth · helical structures · lead · tungsten

[1] a) C. M. Lieber, *Solid State Commun.* **1998**, *107*, 607; b) A. P. Alivisatos, *Science* **1996**, *271*, 933.
[2] Y. Xia, P. Yang, Y. Sun, Y. Wu, B. Mayer, B. Gates, Y. Yin, F. Kim, H. Yan, *Adv. Mater.* **2003**, *15*, 353.
[3] S. H. Yu, B. Liu, M. S. Mo, J. H. Huang, X. M. Liu, Y. T. Qian, *Adv. Funct. Mater.* **2003**, *13*, 639.
[4] Z. W. Pan, Z. R. Dai, Z. L. Wang, *Science* **2001**, *291*, 1947.
[5] X. Wang, X. M. Sun, D. Yu, B. S. Zou, Y. Li, *Adv. Mater.* **2003**, *15*, 1442.
[6] a) H. Yang, N. Coombs, G. A. Ozin, *Nature* **1997**, *386*, 692; b) G. A. Ozin, H. Yang, I. Sokolov, N. Coombs, *Adv. Mater.* **1997**, *9*, 662; c) S. Mann, *Angew. Chem.* **2000**, *112*, 3532; *Angew. Chem. Int. Ed.* **2000**, *39*, 3392; d) S. H. Yu, M. Antonietti, H. Colfen, J. Hartmann, *Nano Lett.* **2003**, *3*, 379.
[7] J. Y. Lao, J. G. Wen, Z. F. Ren, *Nano Lett.* **2002**, *2*, 1287.
[8] a) J. T. Hu, T. W. Odom, C. M. Lieber, *Acc. Chem. Res.* **1999**, *32*, 435; b) A. M. Morales, C. M. Lieber, *Science* **1998**, *279*, 208; c) X. F. Duan, C. M. Lieber, *Adv. Mater.* **2000**, *12*, 298.
[9] a) J. Goldberger, R. R. He, Y. F. Zhang, S. W. Lee, H. Q. Yan, H. J. Choi, P. D. Yang, *Nature* **2003**, *422*, 599; b) R. Fan, Y. Y. Wu, D. Y. Li, M. Yue, A. Majumdar, P. D. Yang, *J. Am. Chem. Soc.* **2003**, *125*, 5254.
[10] a) Z. R. Tian, J. A. Voigt, J. Liu, B. Mckenzie, M. J. Mcdermott, *J. Am. Chem. Soc.* **2002**, *124*, 12954; b) D. Kuang, A. Xu, Y. Fang, H. Liu, C. Frommen, D. Fenke, *Adv. Mater.* **2003**, *15*, 1747.
[11] a) W. A. Lopes, H. M. Jaeger, *Nature* **2001**, *414*, 735; b) X. Chen, Z. Chen, N. Fu, G. Lu, B. Yang, *Adv. Mater.* **2003**, *15*, 1413.
[12] a) D. D. Archibald, S. Mann, *Nature* **1993**, *364*, 430; b) S. Mann, G. A. Ozin, *Nature* **1996**, *382*, 313; c) for a review, see: H. Cölfen, S. Mann, *Angew. Chem.* **2003**, *115*, 2452; *Angew. Chem. Int. Ed.* **2003**, *42*, 2350 and references therein; L. A. Estroff, A. D. Hamilton, *Chem. Mater.* **2001**, *13*, 3227.
[13] K. Nitsch, M. Nikl, S. Ganschow, P. Reiche, R. Uecker, *J. Cryst. Growth* **1996**, *165*, 163.
[14] K. Tanji, M. Ishii, Y. Usuki, M. Kobayashi, K. Hara, H. Takano, *J. Cryst. Growth* **1999**, *204*, 505.
[15] a) P. Lecoq, I. Dafinei, E. Auffray, M. V. Korzhik, V. B. Pavlenko, A. A. Fedorov, A. N. Annencov, V. L. Kostyllev, V. D. Ligun, *Nucl. Instrum. Methods Phys. Res. Sect. A* **1995**, *365*, 291.
[16] A. A. Kaminskii, H. J. Eichler, K. Ueda, N. V. Klassen, B. S. Redkin, L. E. Li, J. Findeisen, D. Jaque, J. Garcia-Sole, J. Fernandez, R. Balda, *Appl. Opt.* **1999**, *38*, 4533.
[17] C. H. An, K. B. Tang, G. Z. Shen, C. R. Wang, Y. T. Qian, *Mater. Lett.* **2002**, *57*, 565.
[18] S. H. Yu, M. Antonietti, H. Cölfen, M. Giersig, *Angew. Chem.* **2002**, *114*, 2462; *Angew. Chem. Int. Ed.* **2002**, *41*, 2356.

[19] X. L. Hu, Y. J. Zhu, *Langmuir* **2004**, *20*, 1521.
[20] K. Nitsch, M. Nikl, M. Rodova, S. Santucci, *Phys. Status Solidi A*, **2000**, *179*, 261.
[21] a) R. L. Penn, J. F. Banfield, *Geochim. Cosmochim. Acta* **1999**, *63*, 1549; b) R. L. Penn, J. F. Banfield, *Science* **1998**, *281*, 969.
[22] Z. Y. Tang, N. A. Kotov, M. Giersig, *Science* **2002**, *297*, 237.
[23] Y. W. Jun, M. F. Casula, J. H. Sim, S. Y. Kim, J. Cheon, A. P. Alivisatos, *J. Am. Chem. Soc.* **2003**, *125*, 15981.
[24] D. Kuang, A. Xu, Y. Fang, H. Liu, C. Frommen, D. Fenske, *Adv. Mater.* **2003**, *15*, 1747.
[25] Y. Ma, L. Qi, J. Ma, H. Cheng, *Cryst. Growth Des.* **2004**, *2*, 351.
[26] M. Crane, R. L. Frost, P. A. Williams, J. T. Kloprogge, *J. Raman Spectrosc.* **2002**, *33*, 62.
[27] S. D. Ross, *Inorganic Infrared and Raman Spectra*, McGraw-Hill, Maidenhead, **1972**.
[28] a) K. Polak, M. Nikl, K. Nitsch, M. Kobayashi, M. Ishii, Y. Usuki, O. Jarolimek, *J. Lumin.* **1997**, *72–74*, 781; b) M. Nikl, P. Strakova, K. Nitsch, V. Petricek, V. Mucka, O. Jarolimek, J. Novak, P. Fabeni, *Chem. Phys. Lett.* **1998**, *291*, 300.

